# A VIRTUAL MIMO CHANNEL REPRESENTATION AND APPLICATIONS

Akbar M. Sayeed

Electrical and Computer Engineering
University of Wisconsin-Madison
1415 Engineering Drive
Madison, WI 53706

## ABSTRACT

*A key to maximal exploitation of MIMO (multiple-input multiple-output) systems is a fundamental understanding of the interaction between the underlying complex physical scattering environment and the space-time signal space. In time- and frequency-selective MIMO (space-time) channels, this interaction happens in time, frequency and space. We present a four-dimensional Karhunen-Loeve-like virtual representation for space-time channels that captures such interaction and exposes the intrinsic degrees of freedom in the channel. The virtual representation is a Fourier series dictated by the finite array apertures, signaling duration and bandwidth and corresponds to a uniform, fixed sampling of the angle-delay-Doppler scattering space. It provides a much-needed connection between the two existing (extreme) modeling approaches — idealized statistical models and detailed physical (ray tracing) models. In particular, it yields a simple geometric interpretation of the effects of physical scattering on channel statistics and capacity. We discuss various insights into the structure of space-time channels afforded by the virtual representation as well its application in capacity assessment, spatial multiplexing and space-time code design.*

## 1. INTRODUCTION

The capacity and diversity afforded by a time- and frequency-selective MIMO (space-time) fading channel is due to the distribution of scatterers in space and the relative motion of the transmitter and receiver arrays. The distribution of scatterers and antenna array parameters determine the statistics of the space-time channel, which in turn determine its capacity and diversity. Accurate modeling of the scattering environment is thus paramount to realizing the full potential of antenna arrays. A key to reliable communication is a fundamental understanding of interaction between the channel and the signal space. An *effective channel representation* that captures the essence of such interaction is all this is needed from a communication viewpoint. In space-time channels, this interaction happens in four signal space dimensions: time, frequency, and the spatial dimensions at the transmitter and receiver.

In this paper, we propose a new virtual representation for space-time channels that captures the essence of channel-signal space interaction in time, frequency and space. It is a generalization of the virtual representation for narrowband correlated MIMO channels introduced in [1]. Each physical scatterer can be associated with a unique Angle of Departure (AoD), Angle of Arrival (AoA), delay, and Doppler shift. The virtual representation replaces the actual physical scatterers with virtual scatterers associated with fixed uniformly spaced AoD's, AoA's, delays and Doppler shifts on a four-dimensional (4D) grid. The grid spacings in the four dimensions correspond to the resolutions in time, frequency and the two spatial dimensions that are determined by the signaling bandwidth, duration, and array apertures, respectively. The virtual representation is a 4D Fourier series representation for $\boldsymbol{H}(t, f)$ and yields many powerful insights. First, under the assumption of uncorrelated physical scattering, $\boldsymbol{H}(t, f)$ is a segment of a 4D wide-sense stationary (WSS) process and the virtual coefficients constitute the corresponding *uncorrelated* spectral representation. Thus, non-vanishing virtual coefficients capture the essential degrees of freedom in the channel in temporal, spectral and spatial dimensions that in turn determine its statistics and capacity. Second, the virtual representation also yields a simple and intuitively appealing interpretation of the effect of scattering environment on capacity [1]. Finally, the representation induces a virtual partitioning of propagation paths that explicitly reveals their contribution to channel capacity and diversity.

The next section presents a general model for space-time channels. Section 3 introduces the virtual representation, including the virtual path partitioning and its implications for channel statistics. Section 4 discusses fundamen-

This research was supported in part by the National Science Foundation under grants CCR-9875805 and CCR-0113385, and the Office of Naval Research under grant N00014-01-1-0825.



0-7803-8140-0/03$17.00 (C) 2003 IEEE

tal dependencies between delay, doppler and angle that are important in characterizing the degrees of freedom. Section 5 shows some illustrative numerical results. Section 6 briefly discusses some applications of the virtual representation in system design.

## 2. A GENERAL MODEL FOR SPACE-TIME CHANNELS

Consider a transmitter array with $P$ elements and a receiver array with $Q$ elements. We are interested in representing the space-time channel over a signaling duration $T$ and two-sided bandwidth $W$. In the absence of noise, the channel equation is

$$\boldsymbol{x}(t) = \int_{-W/2}^{W/2} \boldsymbol{H}(t,f)\boldsymbol{S}(f)e^{j2\pi ft}df, \quad 0 \le t \le T, \quad (1)$$

where $\boldsymbol{s}(t)$ is the $P$-dimensional transmitted signal, $\boldsymbol{S}(f)$ is the Fourier transform of $s(t)$, $\boldsymbol{x}(t)$ is the $Q$-dimensional received signal, and $\boldsymbol{H}(t,f)$ denotes the *time-varying frequency response matrix* coupling the transmitter and receiver elements. We index entries of $\boldsymbol{H}(t,f)$ as $H(i,k;t,f)$ : $i = 0,1,\cdots,Q-1$, $k = 0,1,\cdots,P-1$.

We focus on one-dimensional ULAs of antennas at the transmitter and receiver and consider far-field scattering characteristics. Let $d_T$ and $d_R$ denote the antenna spacings at the transmitter and receiver, respectively. The channel matrix can be described via the array steering and response vectors

$$\begin{aligned} \boldsymbol{a}_T(\theta_T) &= \frac{1}{\sqrt{P}}\left[1,\ e^{-j2\pi\theta_T},\cdots,e^{-j2\pi(P-1)\theta_T}\right]^T \\ \boldsymbol{a}_R(\theta_R) &= \frac{1}{\sqrt{Q}}\left[1,\ e^{-j2\pi\theta_R},\cdots,e^{-j2\pi(Q-1)\theta_R}\right]^T \quad (2) \end{aligned}$$

where $\theta$ is related to the AoA/AoD variable $\varphi$ (measured with respect to the horizontal axis — see Figure 1) as $\theta = d\sin(\varphi)/\lambda = \alpha\sin(\varphi)$, $\lambda$ is the wavelength of propagation, and $\alpha = d/\lambda$ is the normalized antenna spacing. We restrict ourselves to critical ($\lambda/2$) spacing: $\alpha_T = \alpha_R = 0.5$. In this case, there is a one-to-one mapping between $\theta \in [-0.5, 0.5]$ and $\varphi \in [-\pi/2, \pi/2]$. The effect of larger antenna spacings is discussed in detail in [1].

$\boldsymbol{H}(t,f)$ can be generally modeled as

$$\boldsymbol{H}(t,f) = \sum_{n=1}^{N} \beta_n \boldsymbol{a}_R(\theta_{R,n})\boldsymbol{a}_T^H(\theta_{T,n})e^{j2\pi\nu_n t}e^{-j2\pi\tau_n f} \quad (3)$$

which corresponds to propagation over $N$ paths; $\{\theta_{T,n} \in [S_{T-}, S_{T+}] \subset [-0.5, 0.5)\}$ and $\{\theta_{R,n} \in [S_{R-}, S_{R+}] \subset [-0.5, 0.5)\}$ represent the spatial angles (AoDs/AoAs) seen by the transmitter and receiver, respectively, $\{\nu_n \in [-\nu_{DS}, \nu_{DS}]\}$ and $\{\tau_n \in [0, \tau_{DS}]\}$ are the Doppler shifts and delays, respectively, and $\{\beta_n\}$ are the independent complex Gaussian path gains. $\tau_{DS}$ denotes the delay spread, $\nu_{DS}$ denotes the one-sided Doppler spread, and $[S_{T-}, S_{T+}]$ and $[S_{R-}, S_{R+}]$ represent the angular spreads.

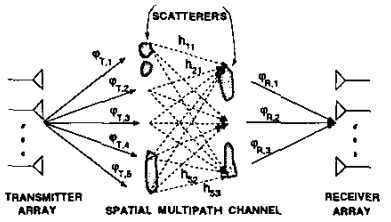


**Fig. 1**. *A schematic illustrating the* **virtual representation** *in the spatial dimension. The virtual angles are fixed a priori and their spacing defines the spatial resolution. The channel is characterized by the virtual coefficients, $\{H_V(q,p) = h_{q,p}\}$, that couple the $P$ virtual transmit angles, $\{\varphi_{T,p}\}$, with the $Q$ virtual receive angles, $\{\varphi_{R,q}\}$.*

## 3. VIRTUAL CHANNEL REPRESENTATION

In (3), each propagation path is associated with an AoD, AoA, delay and Doppler shift which can be arbitrarily distributed within the angular, delay and Doppler spreads. The virtual representation replaces the physical propagation paths with virtual ones corresponding to fixed AoD's, AoA's, delays and Doppler shifts that are determined by the spatial, temporal and spectral resolution afforded by the finite dimensional space-time signal space. The notion of virtual angles is illustrated in Figure 1. The *virtual channel representation* can be expressed as

$$\begin{aligned} \boldsymbol{H}(t,f) &= \sum_{q,p,m,l} H_V(q,p;m,l)\boldsymbol{a}_R(q/Q)\boldsymbol{a}_T^H(p/P) \\ &\quad e^{j2\pi mt/T}e^{-j2\pi lf/W} \quad (4) \end{aligned}$$

corresponding to fixed virtual AoD's, AoA's, delays and Doppler shifts defined as

$$\tilde{\theta}_{T,p} = \frac{p}{P},\ P_- \le p \le P_+,\ \tilde{\theta}_{R,q} = \frac{q}{Q},\ Q_- \le q \le Q_+ \quad (5)$$

$$\tilde{\nu}_m = \frac{m}{T},\ -M \le m \le M,\ \tilde{\tau}_l = \frac{l}{W},\ 0 \le l \le L, \quad (6)$$

where $L = \lceil W\tau_{DS} \rceil$ and $M = \lceil T\nu_{DS} \rceil$ denote the normalized delay and Doppler spreads. $P_- = \lfloor S_{T-}P \rfloor$, $P_+ =$

$\lceil S_{T_+} P \rceil$, $Q_- = \lfloor S_{R_-} Q \rfloor$, and $Q_+ = \lceil S_{R_+} Q \rceil$ represent the normalized angular spreads. The virtual representation is characterized by the coefficients $\{H_V(q,p;m,l)\}$. The transmit/receive virtual angle spacings represent the spatial resolutions that are determined by the array apertures ($\Delta\theta_T = 1/P$ and $\Delta\theta_R = 1/Q$). The virtual Doppler and delay spacings correspond to the spectral and temporal resolutions and are determined by the signaling duration and bandwidth ($\Delta\nu = 1/T$ and $\Delta\tau = 1/W$).

We now address the computation of the virtual representation from $\boldsymbol{H}(t,f)$. Assume WLOG that $P, Q$ are odd and define $\widetilde{P} = (P-1)/2, \widetilde{Q} = (Q-1)/2$. The representation (4) can be decoupled as

$$\begin{aligned} \boldsymbol{H}(t,f) &= \widetilde{\boldsymbol{A}}_R \boldsymbol{H}_V(t,f) \widetilde{\boldsymbol{A}}_T^H \quad (7) \\ \widetilde{\boldsymbol{A}}_R &= [\boldsymbol{a}_R(-\widetilde{Q}/Q), \cdots, \boldsymbol{a}_R(\widetilde{Q}/Q)] \ (Q \times Q) \\ \widetilde{\boldsymbol{A}}_T &= [\boldsymbol{a}_T(-\widetilde{P}/P), \cdots, \boldsymbol{a}_T(\widetilde{P}/P)] \ (P \times P) \quad (8) \end{aligned}$$

where $\widetilde{\boldsymbol{A}}_R$ and $\widetilde{\boldsymbol{A}}_T$ are discrete Fourier transform matrices, as evident from (2) and (5).[1] The matrix $\boldsymbol{H}_V(t,f)$ in (7) is the partial virtual representation with respect to space and can be computed by beamforming in the direction of virtual angles

$$\begin{aligned} \boldsymbol{H}_V(t,f) &= \widetilde{\boldsymbol{A}}_R^H \boldsymbol{H}(t,f) \widetilde{\boldsymbol{A}}_T \\ &= \sum_{l=0}^{L} \sum_{m=-M}^{M} \boldsymbol{H}_V(m,l) e^{j\frac{2\pi mt}{T}} e^{-j\frac{2\pi lf}{W}} \quad (9) \end{aligned}$$

where the second equality further decomposes $\boldsymbol{H}_V(t,f)$ into component matrices $\boldsymbol{H}_V(m,l)$ corresponding to fixed virtual Doppler shifts and delays, which can be computed from $\boldsymbol{H}_V(t,f)$ as

$$\boldsymbol{H}_V(m,l) = \frac{1}{TW} \int_0^T \int_{-W/2}^{W/2} \boldsymbol{H}_V(t,f) e^{-j\frac{2\pi mt}{T}} e^{j\frac{2\pi lf}{W}} dt df. \quad (10)$$

### 3.1. Virtual Path Partitioning

The virtual representation induces a partitioning of propagation paths that is very insightful in determining their contribution to capacity and diversity. Define the following subsets of propagation paths

$$\begin{aligned} S_{T,p} &= \{n : (p-1/2)/P \le \theta_{T,n} < (p+1/2)/P\} \quad (11) \\ S_{R,q} &= \{n : (q-1/2)/Q \le \theta_{R,n} < (q+1/2)/Q\} \quad (12) \\ S_{\nu,m} &= \{n : (m-1/2)/T \le \nu_n < (m+1/2)/T\} \quad (13) \\ S_{\tau,l} &= \{n : (l-1/2)/W \le \tau_n < (l+1/2)/W\} \quad (14) \end{aligned}$$

[1] Note that $\widetilde{\boldsymbol{A}}_R$ and $\widetilde{\boldsymbol{A}}_T$ contain all possible virtual angles, some of which lie outside the angular spreads. $H_V(q,p;m,l)$ will be approximately zero for those angles.

corresponding to transmit spatial resolution, receive spatial resolution, spectral resolution, and temporal resolution. Note that

$$\begin{aligned} \bigcup_p S_{T,p} &= \bigcup_q S_{R,q} = \bigcup_m S_{\nu,m} = \bigcup_l S_{\tau,l} \\ &= \bigcup_{p,q,m,l} S_{T,p} \cap S_{R,q} \cap S_{\nu,m} \cap S_{\tau,l} \\ &= \{1, 2, \cdots, N\}. \quad (15) \end{aligned}$$

Then, the virtual coefficients can be approximated as [3]

$$H_V(q,p;m,l) \approx \sum_{n \in S_{q,p,m,l}} \beta_n. \quad (16)$$

where $S_{q,p,m,l} = S_{T,p} \cap S_{R,q} \cap S_{\nu,m} \cap S_{\tau,l}$. Equation (16) states that $H_V(q,p;m,l)$ is determined by the sum of gains of all paths that lie in $S_{q,p,m,l}$. The approximation in (16) get more accurate with increasing $P, Q, T$ and $W$.

### 3.2. Channel Statistics

One of the most important characteristics of the virtual representation is that $\{H_V(q,p;m,l)\}$ are approximately uncorrelated under the assumption of uncorrelated path gains: $\mathrm{E}[\beta_n \beta_{n'}^*] = \sigma_n^2 \delta_{n-n'}$ where $\delta_n$ denotes the kronecker delta function and $\sigma_n^2$ is the power in each path. This observation is directly evident from (16)

$$\begin{aligned} &\mathrm{E}[H_V(q,p;m,l) H_V^*(q',p';m',l')] \approx \\ &\left[ \sum_{n \in S_{q,p,m,l}} \sigma_n^2 \right] \delta_{q-q'} \delta_{p-p'} \delta_{m-m'} \delta_{l-l'}. \quad (17) \end{aligned}$$

Thus, from (16) we have

$$\begin{aligned} R_H(\Delta i, \Delta k; \Delta t, \Delta f) &= \mathrm{E}[H(i,k;t,f) H^*(i',k';t',f')] \\ &\approx \sum_{q,p,m,l} \sigma_{q,p,m,l}^2 e^{-j\frac{2\pi q \Delta i}{Q}} e^{j\frac{2\pi p \Delta k}{P}} \\ &\quad e^{j\frac{2\pi m \Delta t}{T}} e^{-j\frac{2\pi l \Delta f}{W}}, \quad (18) \end{aligned}$$

$\Delta i = i - i'$, $\Delta k = k - k'$, $\Delta t = t - t'$, $\Delta f = f - f'$, and

$$\begin{aligned} \sigma_{q,p,m,l}^2 &= \mathrm{E}[|H_V(q,p;m,l)|^2] \\ &\approx \sum_{n \in S_{q,p,m,l}} \sigma_n^2 \quad (19) \end{aligned}$$

is the power in $H_V(q,p;m,l)$ and the approximation in (19) is due to virtual path partitioning. Relation (18) yields the insightful conclusion that under the assumption of uncorrelated path gains, $\boldsymbol{H}(t,f)$ is a segment of a 4D WSS process in the two spatial dimensions, time and frequency,

and $\{H_V(q,p;m,l)\}$ constitute the corresponding uncorrelated spectral representation. Furthermore, (19) states that the power in $H_V(q,p;m,l)$ is equal to the sum of the powers in the paths that lie in $S_{q,p,m,l}$. We note that the extent of channel correlation is inversely proportional to the support of the dominant virtual coefficients.

## 4. DEPENDENCIES IN DELAY, DOPPLER AND ANGLE

From (4) we may conclude that the total independent degrees of freedom in the space-time channel are

$$N_{ST} = (Q_+ - Q_- + 1)(P_+ - P_- + 1)(L+1)(2M+1) \tag{20}$$

where $(Q_+ - Q_- + 1)(P_+ - P_- + 1)$ represents the degrees of freedom in angle and $(L+1)(2M+1)$ represents the degrees of freedom in delay and Doppler. We now use virtual path partitioning to demonstrate fundamental dependencies between angle, delay and Doppler that cause the essential degrees of freedom to be less than the upperbound in (20).

The dependencies are due to the fact that the delay and Doppler spreads are proportional to the angular spreads. For given $(q,p)$, $H_V(q,p;m,l)$ is non-vanishing over $(l,m)$ between

$$L_{-(q,p)} = \left\lfloor \left[ \min_{S_{q,p}} \tau_n \right] W \right\rfloor, \quad L_{+(q,p)} = \left\lceil \left[ \max_{S_{q,p}} \tau_n \right] W \right\rceil \tag{21}$$

$$M_{-(q,p)} = \left\lfloor \left[ \min_{S_{q,p}} \nu_n \right] T \right\rfloor, \quad M_{+(q,p)} = \left\lceil \left[ \max_{S_{q,p}} \nu_n \right] T \right\rceil \tag{22}$$

where $S_{q,p} = S_{R,q} \cap S_{T,p}$. Consequently, (4) can be refined to limit the ranges of $l$ and $m$ as a function of $(q,p)$ as above to reflect the essential degrees of freedom

$$N_{ST,ess} = \sum_{q,p} \sum_{l=L_{-(q,p)}}^{L_{+(q,p)}} \sum_{m=M_{-(q,p)}}^{M_{+(q,p)}} \leq N_{ST}. \tag{23}$$

Note that $N_{ST,ess} = N_{ST}$ in (20) if and only if $(L_+ - L_- + 1)(M_+ - M_- + 1) = (L+1)(2M+1)$ for all $(q,p)$ which would seldom be true particularly for channels that are *underspread* ($\tau_{\mathrm{DS}}\nu_{\mathrm{DS}} \ll 1$). This is because time/frequency selectivity exhibited by $H_V(q,p;t,f)$ depends on the spatial resolution: higher resolutions would result in less selectivity whereas lower resolutions will result in higher selectivity. A SISO channel will exhibit maximum time/frequency selectivity.

Figure 2 illustrates a simple scattering geometry to quantify the dependencies. Consider a single scattering cluster

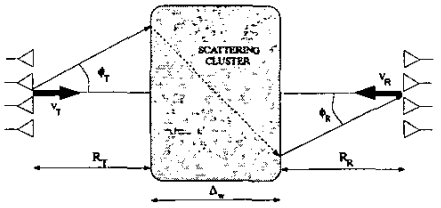


**Fig. 2.** *An illustration of the dependence of delay and Doppler shift on the virtual transmit and receive angles.*

at a distance $R_T$ from the transmitter and $R_R$ from the receiver. Suppose that $v_T$ denotes the relative speed between the transmitter and the cluster and $v_R$ the relative speed between the receiver and the cluster. Let $\Delta_T$ and $\Delta_R$ denote the angular spreads, and $\Delta_w$ the "width" of the cluster. Via simple geometric considerations, $\tau$ and $\nu$ can be estimated for any given $(\theta_R, \theta_T)$ as

$$\tau = \sqrt{\Delta_w^2 + |R_T\theta_T/\alpha_T - R_R\theta_R/\alpha_R|^2}/c \tag{24}$$

$$\nu = f_{\max,\mathrm{T}}\sqrt{1 - \theta_T{}^2/\alpha_T^2} + f_{\max,\mathrm{R}}\sqrt{1 - \theta_R{}^2/\alpha_R^2} \tag{25}$$

where $c$ denotes the speed of light, $f_{\max,\mathrm{T}} = v_T/c$ and $f_{\max,\mathrm{R}} = v_R/c$. We note the expression for $\tau$ is strictly a lowerbound since multiple bounces [2] within the cluster may result in longer delays.

## 5. ILLUSTRATIVE NUMERICAL RESULTS

We now present some numerical results to illustrate the effect of time/frequency selectivity on capacity and the effect of number of antennas on time/frequency selectivity of the channel. We simulated a single scattering cluster, as in Figure 2, with angular spreads of $\Delta_T = \Delta_R = 2\pi/3$ centered at $(\varphi_T, \varphi_R) = (0,0)$. We considered $N = 100$ propagation paths. We first generated $N$ pairs of angles, $\{\varphi_{R,n}, \varphi_{T,n}\}$, uniformly distributed within the angular spreads to fix the scatterer positions. To simulate time/frequency selectivity, we considered a temporal signal space with $N_o = TW = 65$ dimensions. We simulated three types of channels. **CH 1** (flat): $R_T = R_R = 1000$m, $f_{\max,\mathrm{R}} = f_{\max,\mathrm{T}} = 50$ Hz, $W = 1$ MHz, $T = 65\mu s$. **CH 2** (medium selective): $R = 8000$m, $f_{\max} = 400$ Hz, $W = 1$ MHz, $T = 65\mu s$. **CH 3** (highly selective): $R = 8000$m, $f_{\max} = 400$ Hz, $W = 10$ MHz, $T = 6.5\mu s$. $\Delta w = 100$m in all cases. Both **CH 1** and **CH 2** have the same $T$ and $W$ but **CH 2** has larger delay and Doppler spreads and is thus more selective. **CH 3** has the same delay and Doppler spreads but is even more selective than **CH 2** due to larger $W$ (delay diversity is easier to exploit in this case). Channel realizations were generated using

(3) via iid complex Gaussian $\{\beta_n\}$. Each realization was normalized to yield $\sum \beta_n^2 = PQ$.

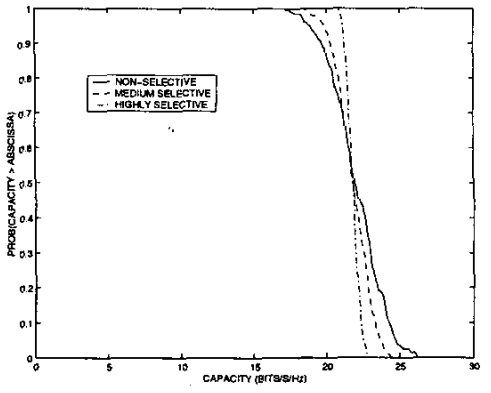


**Fig. 3**. *Comparison of the three channels illustrating the effect of time/frequency selectivity on outage capacity.*

Figure 3 illustrates the effect of time/frequency selectivity on outage capacity for $P = Q = 4$ antennas. The (normalized) capacity (in bits/s/Hz) was numerically computed using 200 independent channel realizations at an SNR of 20dB (see [3] for details). As evident, the outage capacity curves get steeper (higher diversity) as the channel gets more selective. The ergodic capacity of all three channels is approximately 21.8 bits/s/Hz. Note that this is consistent with the experimental results reported in [2] and in disagreement with analytical results reported in [4] which suggested that increased delay spread can increase ergodic capacity. We can prove using our framework that frequency selectivity does not increase ergodic capacity and this apparent inconsistency with the conclusion of [4] is due to an incorrect interpretation of results in [4] (see [5] for details).

Figure 4 illustrates the dependencies between angle, delay and Doppler. **CH 2** was simulated using $P = Q = 2$ and $P = Q = 4$ antennas. The figure shows contour plots of a subset of $\sigma^2_{q,p,m,l}$ as a function of $(m, l)$ for a representative $(q, p)$. It is evident that the delay-Doppler spread *decreases* in the virtual spatial domain for larger number of antennas, as predicted by our analysis. The number of significant $\sigma^2_{q,p,m,l}$ provides an estimate for $N_{ST,eff}$ in (23). Our simulations yielded $N_{ST,eff}/QP = 4.5$ in the 2-antenna case and 2.75 in the 4-antenna case, confirming that time and frequency selectivity decreases in the virtual spatial domain as the number of antennas increases.

## 6. APPLICATIONS

We now briefly outline some areas of system design for doubly selective correlated MIMO channels in which the virtual representation has been successfully applied.

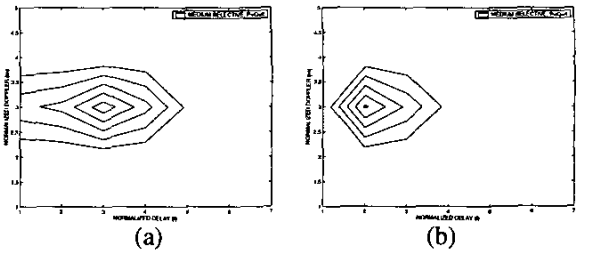


**Fig. 4**. *Contour plots of the powers in a subset of non-vanishing virtual delay-Doppler coefficients for* **CH 2** *for a representative virtual angle pair $(q, p)$. (a) $Q = P = 2$. (b) $P = Q = 4$.*

**Channel Estimation.** In [6], we address the problem of transmit signal design for MMSE estimation of narrowband correlated MIMO channels. For a $Q \times P$ MIMO matrix $\boldsymbol{H}$, there are $PQ$ parameters to be estimated in general. However, for correlated channels, the degrees of freedom in the channel are captured by a much smaller set of uncorrelated virtual coefficients that are dominant (large compared to the background noise). The optimal estimator takes a simple form in the virtual domain: The transmitter sequentially sends beams in different virtual transmit directions and the corresponding columns of the virtual MIMO matrix are estimated at the receiver. The optimal power allocation in different transmit directions is determined by a waterfilling criteria which determines the dominant virtual coefficients that need to be estimated at any given SNR. In particular, at high SNR all transmit beams within the angular spread get power. Whereas, at low SNR, only a single transmit direction with the strongest coupling to the receiver gets all the power. The notion of dominant virtual coefficients is also important in space-time code design and non-coherent communication.

**Spatial Multiplexing and Space-Time Code Design.** In [7, 8], we leverage the virtual representation for developing spatial multiplexing (BLAST-type) techniques and space-time codes for correlated MIMO channels. The uncorrelated nature of the virtual representation greatly simplifies the pairwise error probability analysis to characterize the diversity and coding gains. In particular, unlike i.i.d. channels, the code performance is governed by the eigenvalues of a matrix that depends on the both the channel covariance matrix and error-covariance matrix of the codewords. Using the virtual representation, an explicit characterization of the eigenvalues is provided that naturally suggests a coding framework for correlated channels based on linear precoding. Performance analysis shows that codes

designed for i.i.d. channels can degrade drastically in correlated scenarios, and that significant improvement in performance is possible by exploiting the structure of correlated channels in the virtual domain.

**Channel Capacity and Capacity Scaling.** It is well-known that for i.i.d. channels, the optimum input for maximizing coherent capacity (when the channel is known at the receiver only) is uncorrelated across antennas and the power should be equally distributed amongst the antennas [9]. However, for correlated channels this has been an open problem which has been solved in some specific cases [10]. In a recent work, Liang and Veeravalli[2] have shown that in the virtual domain, regardless of the channel correlation, the optimal input is always uncorrelated! The optimal power allocation in the different virtual transmit directions is determined by a waterfilling criterion. This is a powerful result that applies to arbitrary number of antennas and greatly facilitates capacity analysis. In [5], we investigate the important issue of capacity scaling. Consider an equal number of transmit and receive antennas. It is well-known that i.i.d. channels promise a dramatic linear increase in coherent capacity with the number of antennas. However, i.i.d. channels seldom occur in practice, particularly for feasible antenna spacings and moderately large number of antennas. When is such scaling possible in realistic scattering environments? In [5], motivated by physical considerations, we propose a $D$-connected model for the virtual MIMO matrix consisting of $D$ non-vanishing diagonals. The connectivity parameter $D$ captures the richness of scattering and quantifies the number of receive virtual angles that couple with each virtual transmit angle, and vice versa.[3] We show that linear capacity scaling is possible if $D$ scales linearly with the number of antennas. Using virtual path partitioning, we relate this result to the number of resolvable propagation paths: linear capacity scaling is possible if the number of resolvable paths increases *quadratically* with the number of antennas. A linear growth in the number of paths with the number of antennas corresponds to fixed $D$ and results in capacity saturation. For a given number of propagation paths $N$, there is no point in deploying more than $N$ antennas.

**Wireless Networks.** We note in closing the most far-reaching application of the virtual representation framework for capacity assessment and information routing in multi-hop wireless networks. This ongoing research is inspired by an intriguing connection between *point-to-point communication via intermediate scatterers* in a physical MIMO wireless link and *source-destination communication via intermediate (relaying) nodes* in a multi-hop wireless network. This "node $\leftrightarrow$ scatterer" analogy can be made precise and has deep and wide ranging implications for the design of multi-hop wireless networks.

[2]To be presented at Asilomar 2003.

[3]It includes the i.i.d. channel as a special case.

## 7. REFERENCES


[1] A. M. Sayeed, "Deconstructing multi-antenna fading channels," *IEEE Trans. Signal Processing*, pp. 2563–2579, Oct. 2002.

[2] A. F. Molisch, M. Steinbauer, M. Toeltsch, E. Bonek, and R. S. Thomä, "Capacity of MIMO systems based on measured wireless channels," *IEEE J. Selec. Areas. Commun.*, pp. 561–569, Apr. 2002.

[3] A. M. Sayeed and V. V. Veeravalli, "A virtual representation for time and frequency selective mimo channels," *to be submitted*, 2003.

[4] H. Bolcskei, D. Gesbert, and A. J. Paulraj, "On the capacity of OFDM-based spatial multiplexing systems," *IEEE Tran. Commun.*, pp. 225–234, Feb. 2002.

[5] K. Liu, V. Raghavan, and A. M. Sayeed, "Capacity scaling and spectral efficiency in wideband correlated MIMO channels," *to appear in the IEEE Trans. Inf. Th. (special issue on MIMO systems)*, 2003.

[6] J. Kotecha and A. M. Sayeed, "Optimal signal design for estimation of correlated MIMO channels," *to appear in the IEEE Trans. Signal Processing*, 2003.

[7] Z. Hong, K. Liu, R. Heath, and A. Sayeed, "Spatial multiplexing in correlated fading via the virtual channel representation," *IEEE J. Select. Areas Commun. (special issue on MIMO systems)*, pp. 856–866, June 2003.

[8] K. Liu and A. M. Sayeed, "Space-time D-block codes via the virtual MIMO channel representation," *to appear in the IEEE Trans. Wireless Commun.*, 2003.

[9] E. Telatar, "Capacity of multi-antenna Gaussian channels," *AT& T-Bell Labs Internal Tech. Memo.*, June 1995.

[10] A. Goldsmith, S. Jafar, N. Jindal, and S. Vishwanath, "Capacity limits of MIMO channels," *IEEE J. Selec. Areas Commun. (special issue on MIMO systems)*, pp. 684–702, June 2003.